International Journal of Modern Physics C
Vol. 15, No. 9 (2004) 1197–1213

World Scientific
www.worldscientific.com

NEW LATTICE KINETIC SCHEMES FOR INCOMPRESSIBLE VISCOUS FLOWS

Y. PENG, C. SHU*, Y. T. CHEW and H. W. ZHENG

Department of Mechanical Engineering
National University of Singapore
10 Kent Ridge Crescent, Singapore 119260
**mpeshuc@nus.edu.sg*

Received 16 April 2004
Revised 27 April 2004

A new two-dimensional lattice kinetic scheme on the uniform mesh was recently proposed by Inamuro, based on the standard lattice Boltzmann method (LBM). Compared with the standard LBM, this scheme can easily implement the boundary condition and save computer memory. In order to remove the shortcoming of a relatively large viscosity at a high Reynolds number, a first-order derivative term is introduced in the equilibrium density distribution function. However, the parameter associated with the derivative term is very sensitive and was chosen in a narrow range for a high Reynolds number case. To avoid the use of the derivative term while removing the shortcoming of a relatively large viscosity, new lattice kinetic schemes are proposed in this work following the original lattice kinetic scheme. In these new lattice kinetic schemes, the derivative term is dropped out and the difficulty of the relatively large viscosity is eased by controlling the time step δt or sonic speed c_s. To validate these new lattice kinetic schemes, the numerical simulations of the two-dimensional square driven cavity flow at Reynolds numbers from 100 to 1000 are carried out. The results using the new lattice kinetic schemes are compared with the benchmark data.

Keywords: Lattice kinetic scheme; lattice Boltzmann method; Taylor series expansion; least square optimization; driven cavity flow.

1. Introduction

In recent years, the lattice Boltzmann method (LBM) has been developed into an alternative promising method for fluid mechanics. It has been widely used in many kinds of complex flows such as the turbulent flow, multiphase flow and micro-flow.[1] However, there is still some space left for improvement. One is for the collision model. The Bhatnagar–Gross–Krook (BGK) model with a single relaxation time is usually used for the collision term. The shortcomings of the BGK model are pointed out in the works of d'Humieres[2] and Lallemand and Luo.[3] The other is for

*Corresponding author.

the boundary condition. The bounce-back scheme in the LBM was originally taken from the lattice gas cellular automata (LGCA) method. Although this heuristic scheme is very simple to implement, it is found to be only of the first order in the numerical accuracy at boundaries.[4,5] In order to improve the numerical accuracy, other boundary treatments have been proposed. It appears, however, that the extension of these treatments to arbitrary boundary geometries is difficult. Chen *et al.*[6] proposed a new boundary condition using a second-order extrapolation scheme of distributions in the flow to obtain unknown particle distribution functions on boundaries. When flow problems with complex geometries, especially in three dimensions, are encountered, the determination of unknown particle directions is troublesome. All these implementations are not so direct because on boundaries, macroscopic variables, not density distributions, are given.

Inverse mapping from macroscopic variables to density distributions is not straightforward as the mapping from density distributions to macroscopic variables. In relation to these two difficulties, a lattice kinetic scheme for incompressible viscous flows was developed by Inamuro.[7] It is based on the idea that if the dimensionless relaxation time in the LBM with the BGK model is set to unity, macroscopic variables can be calculated without the density distribution and the scheme becomes very similar to kinetic schemes. By merging the LBM with kinetic schemes, one may further improve the LBM. This scheme can save memory because there is no need to store the density distribution. The implementation of the boundary condition is very easy since on boundaries, only macroscopic variables, not density distributions, are needed as for the conventional Navier–Stokes (NS) solvers. This feature is very different when flow problems with complex geometries are solved.

However, since this scheme is in the early stage of development, it still needs some improvements. We found that there is a first-order derivative term in the equilibrium density distribution function. This term is introduced so as to remove the relatively large viscosity at a high Reynolds number. Although the first-order derivative term can be approximated by the algebraic relation between the particle velocity and the corresponding macroscopic variables on uniform grids, this relation would break down if used on the arbitrary mesh. Arbitrary meshes are often favored for practical applications and the conventional finite difference approximation and coordinate transformation have to be used. On one hand, compared with the equilibrium density distribution function used by the conventional LBM, it is more complicated. On the other hand, if the finite difference is used to approximate derivatives on the arbitrary mesh, numerical errors will arise, especially at high Reynolds numbers where a large number of grids are clustered near the boundary that may lead to numerical instability.

We aim to propose new lattice kinetic schemes, whose equilibrium distribution functions do not have any derivative term while the relatively large viscosity can be avoided at a high Reynolds number. Through the analysis of the original lattice kinetic scheme, we found that by changing δt or c_s according to the Reynolds

number, the difficulty of the relatively large viscosity can be removed while there is no need to introduce the first-order derivative term into equilibrium density distribution functions. Changing δt can be easily attained by extending the original lattice kinetic scheme to be used on the arbitrary mesh[8]; changing c_s is realized by constructing a new particle velocity model, which has a variable c_s. Detailed explanation about these two methods will be given in the methodology part. Based on this study, two new lattice kinetic schemes are proposed in this paper.

In order to validate our new lattice kinetic schemes, numerical simulations of the square driven cavity flow are carried out and compared with available data.

2. Methodology

Our new lattice kinetic schemes are based on the original lattice kinetic scheme proposed by Inamuro.[7] Before introducing our new lattice kinetic schemes, we will give a brief description about the original lattice kinetic scheme.

2.1. *Original lattice kinetic scheme*

The evolution equation for the density distribution $f_\alpha(\mathbf{x}, t)$ in two dimensions with the particle velocity $\mathbf{e}_\alpha$ can be written as:

$$f_\alpha(\mathbf{x}, t+\delta t) = f_\alpha(\mathbf{x}-\mathbf{e}_\alpha\delta t, t) - \frac{f_\alpha(\mathbf{x}-\mathbf{e}_\alpha\delta t, t) - f_\alpha^{\mathrm{eq}}(\mathbf{x}-\mathbf{e}_\alpha\delta t, t)}{\tau}, \quad \alpha = 0, 1, \ldots, N, \tag{1}$$

where τ is the single relaxation time; f_α^{eq} is the corresponding equilibrium density distribution function; δt is the time step and N is the number of discrete particle velocities. On the uniform grids, δt is chosen so that the particles travel one-lattice spacing during this time. When the particle velocity model D2Q9 ($DnQm$ means m speed model in n dimensions), which is defined as:

$$\mathbf{e}_\alpha = \begin{cases} 0, & \alpha = 0, \\ \left(\cos\left[\dfrac{(\alpha-1)\pi}{2}\right], \sin\left[\dfrac{(\alpha-1)\pi}{2}\right]\right), & \alpha = 1, 2, 3, 4, \\ \sqrt{2}\left(\cos\left[\dfrac{(\alpha-5)\pi}{2}+\dfrac{\pi}{4}\right], \sin\left[\dfrac{(\alpha-5)\pi}{2}+\dfrac{\pi}{4}\right]\right), & \alpha = 5, 6, 7, 8, \end{cases} \tag{2}$$

is used, a suitable equilibrium density distribution function for this model is given by:

$$f_\alpha^{\mathrm{eq}} = w_\alpha \rho \left[1 + 3\mathbf{e}_\alpha \cdot \mathbf{V} + \frac{9(\mathbf{e}_\alpha \cdot \mathbf{V})^2}{2} - \frac{3\mathbf{V}^2}{2}\right], \tag{3}$$

where $w_0 = 4/9$, $w_\alpha = 1/9$ for $\alpha = 1, 2, 3, 4$, $w_\alpha = 1/36$ for $\alpha = 5, 6, 7, 8$. The macroscopic density ρ and fluid velocity $\mathbf{V}$ are calculated in terms of density

distributions as:

$$\rho = \sum_{\alpha=0}^{8} f_\alpha \,, \qquad \mathbf{V} = \frac{1}{\rho} \sum_{\alpha=0}^{8} f_\alpha \mathbf{e}_\alpha \,. \tag{4}$$

The pressure p is related to the density by:

$$p = \frac{\rho}{3} \tag{5}$$

and the kinematic viscosity υ is given by:

$$\upsilon = \left(\tau - \frac{1}{2}\right) c_s^2 \delta t \,. \tag{6}$$

When the dimensionless relaxation time τ in Eq. (1) is set to unity, we obtain

$$f_\alpha(\mathbf{x}, t + \delta t) = f_\alpha^{\mathrm{eq}}(\mathbf{x} - \mathbf{e}_\alpha \delta t, t) \,. \tag{7}$$

Then using Eq. (4), we can get

$$\begin{aligned} \rho(\mathbf{x}, t + \delta t) &= \sum_{\alpha=0}^{8} f_\alpha^{\mathrm{eq}}(\mathbf{x} - \mathbf{e}_\alpha \delta t, t), \rho(\mathbf{x}, t + \delta t)\mathbf{V}(\mathbf{x}, t + \delta t) \\ &= \sum_{\alpha=0}^{8} f_\alpha^{\mathrm{eq}}(\mathbf{x} - \mathbf{e}_\alpha \delta t, t)\mathbf{e}_\alpha \,. \end{aligned} \tag{8}$$

By using Eqs. (3) and (8), one can calculate the density and fluid velocity without using density distributions. The pressure is obtained with Eq. (5) and the kinematic viscosity is given by:

$$\upsilon = \frac{1}{2} c_s^2 \delta t = \frac{1}{6} \delta t \,. \tag{9}$$

This may yield a relatively large viscosity. δt has to be very small at a high Reynolds number, which implies that a large lattice size is needed when uniform grids are used.

In order to remove this shortcoming, Inamuro[7] used the idea that one can flexibly choose the equilibrium density distribution function f_α^{eq} as long as macroscopic equations recover NS equations.[9] The following equilibrium density distribution function is taken

$$f_\alpha^{\mathrm{eq}} = w_\alpha \rho \left[1 + 3\mathbf{e}_\alpha \cdot \mathbf{V} + \frac{9(\mathbf{e}_\alpha \cdot \mathbf{V})^2}{2} - \frac{3\mathbf{V}^2}{2} + A\delta t \left(\frac{\partial u_\delta}{\partial x_\gamma} + \frac{\partial u_\gamma}{\partial x_\delta}\right) e_{\alpha\delta} e_{\alpha\gamma}\right] . \tag{10}$$

The kinematic viscosity is given by:

$$\upsilon = \left(\frac{1}{6} - \frac{2}{9} A\right) \delta t \,. \tag{11}$$

By adjusting the coefficient A, a smaller lattice size can be used at a high Reynolds number. The systems (8) and (10) are called the original lattice kinetic scheme.

2.2. *New lattice kinetic schemes*

From the above derivation, we found that if the derivative term is not introduced in the equilibrium density distribution function, the kinematic viscosity is written as $\upsilon = (1/2)c_s^2\delta t$ and this will yield a relatively large viscosity on uniform grids. This means that at a high Reynolds number, a large lattice size has to be used (δt has to be very small). Take D2Q9 and Re = 1000 as an example. The kinematic viscosity is υ = Ma/Re (reference length is taken as 1 for simplicity). If Ma is chosen to be 0.1, δt will be 6 Ma/Re. This means that the grid size in each direction has to be 1667 and this large grid size is time consuming and requires a large amount of computer memory for numerical simulation. This is why the first-order derivative term is introduced in the equilibrium density distribution function in the original lattice kinetic scheme. The derivative of variables in Eq. (10) can be approximated by:

$$\frac{\partial \phi}{\partial x_\gamma} \approx \frac{1}{6\delta x} \sum_{i=1}^{9} e_{i\gamma} \phi(\mathbf{x} + \mathbf{e}\delta x) \tag{12}$$

on the uniform mesh.

Compared with the equilibrium density distribution function used by the conventional LBM, the form of equilibrium density distribution function expressed by Eq. (10) is more complicated. In addition, in real applications where flow problems with curved boundaries are encountered, the boundary cannot be well defined if uniform grids are used. Even if flows are confined in regular geometries, nonuniform grid is preferred at a high Reynolds number. On the arbitrary mesh, Eq. (12) cannot be used to evaluate derivatives. Therefore, the conventional finite difference approximation has to be used to approximate derivatives and the coordinate transformation may be introduced. As a consequence, a numerical error will arise, especially at a high Reynolds number, which may lead to numerical instability.

In order to remove the difficulty of the relatively large viscosity without introducing the derivative term, new lattice kinetic schemes are proposed in this paper. They are realized by changing δt or c_s according to the Reynolds number.

2.2.1. *Changing δt*

Changing δt can be easily realized by extending the original lattice kinetic scheme to be used on the arbitrary mesh. Without introducing the derivative term in the equilibrium density distribution function, the kinematic viscosity can be written as $\upsilon = (1/2)c_s^2\delta t$. If the nonuniform grid is used, we can set the minimum δx or δy to be 6 Ma/Re, which causes δt to be 6 Ma/Re. In the meantime, we do not need to use a large number of grid points in each direction. This means that we can control the minimum grid distance according to the Reynolds number and Mach number for a given grid size. This can be well accomplished by the grid generation procedure. In order to realize this, the original lattice kinetic scheme has to be extended to

be used on the arbitrary mesh. This has been done in our previous work.[8] A brief introduction will be given in the following.

Techniques of the Taylor series expansion and least squares optimization are introduced into the original lattice kinetic scheme. Suppose that the calculation point is at the grid point $P(x, y, t)$. As seen from Eq. (8), for the original lattice kinetic scheme, the macroscopic density and velocity can be calculated as the function of $f_\alpha^{\mathrm{eq}}(x - e_{\alpha x}\delta t, y - e_{\alpha y}\delta t, t)$. For a uniform lattice, $\delta x = e_{\alpha x}\delta t$, $\delta y = e_{\alpha y}\delta t$, so $(x - e_{\alpha x}\delta t, y - e_{\alpha y}\delta t)$ is at the grid point and the value of $f_\alpha^{\mathrm{eq}}(\mathbf{x} - \mathbf{e}_\alpha\delta t, t)$ can be easily determined from Eq. (3). In other words, Eq. (8) can be used to update the density and velocity exactly at the grid point. However, for a nonuniform grid, $(x - e_{\alpha x}\delta t, y - e_{\alpha y}\delta t)$ is usually not at the grid point $(x - \delta x, y - \delta y)$. The value of $f_\alpha^{\mathrm{eq}}(\mathbf{x} - \mathbf{e}_\alpha\delta t, t)$ cannot be obtained from Eq. (3) directly since only macroscopic properties, such as the density and flow velocity at every mesh point, are known. As a result, the density and velocity at the new time level cannot be obtained using Eq. (8). In order to get the value of $f_\alpha^{\mathrm{eq}}(\mathbf{x} - \mathbf{e}_\alpha\delta t, t)$, the Taylor series expansion in the spatial direction is applied.

As shown in Fig. 1, for simplicity, the point P represents the calculation point (x_P, y_P, t), points A–H represent the position $(x_P - e_{\alpha x}\delta t, y_P - e_{\alpha y}\delta t, t)$, and points $P_1 - P_8$ represent the position (x_{P_i}, y_{P_i}, t) with $x_{P_i} = x_P - \delta x_i, y_{P_i} = y_P - \delta y_i$. Equation (8) gives

$$\rho(\mathbf{x}, t + \delta t) = \sum_{\alpha=0}^{8} f_\alpha^{\mathrm{eq}}(\mathbf{x}_\alpha, t), \rho(\mathbf{x}, t + \delta t)\mathbf{V}(\mathbf{x}, t + \delta t) = \sum_{\alpha=0}^{8} f_\alpha^{\mathrm{eq}}(\mathbf{x}_\alpha, t)\mathbf{e}_\alpha \quad (13)$$

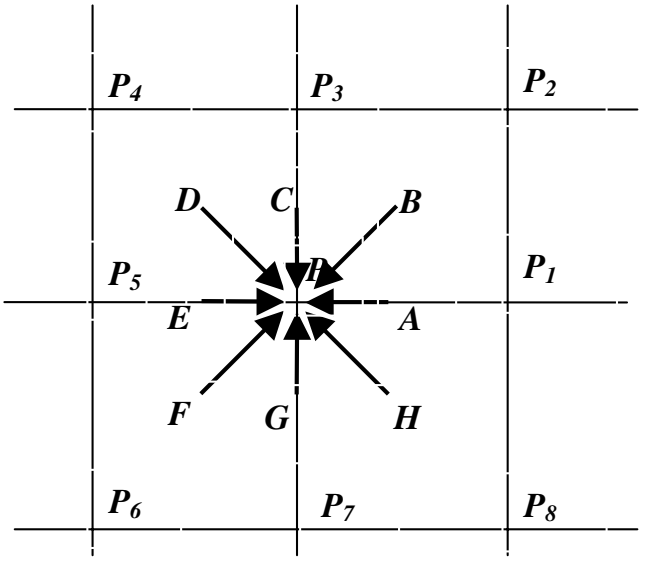

Fig. 1. Configuration at calculation point P.

where $\mathbf{x}_0 = P$, $\mathbf{x}_1 = E$, $\mathbf{x}_2 = F$, $\mathbf{x}_3 = G$, $\mathbf{x}_4 = H$, $\mathbf{x}_5 = A$, $\mathbf{x}_6 = B$, $\mathbf{x}_7 = C$ and $\mathbf{x}_8 = D$.

For the general case, A–H may not coincide with mesh points $P_1 - P_8$. We will take the point F as an example. F may not coincide with the mesh point P_6. Since $f_\alpha^{\mathrm{eq}}(P_6, t)$ is known, we can build the connection between $f_\alpha^{\mathrm{eq}}(F, t)$ and $f_\alpha^{\mathrm{eq}}(P_6, t)$ by using the Taylor series expansion to the second order derivative term, that is

$$\begin{aligned} f_\alpha^{\mathrm{eq}}(P_6, t) = f_\alpha^{\mathrm{eq}}(F, t) &+ \Delta x_{P_6} \frac{\partial f_\alpha^{\mathrm{eq}}(F, t)}{\partial x} + \Delta y_{P_6} \frac{\partial f_\alpha^{\mathrm{eq}}(F, t)}{\partial y} \\ &+ \frac{1}{2}(\Delta x_{P_6})^2 \frac{\partial^2 f_\alpha^{\mathrm{eq}}(F, t)}{\partial x^2} + \frac{1}{2}(\Delta y_{P_6})^2 \frac{\partial^2 f_\alpha^{\mathrm{eq}}(F, t)}{\partial y^2} \\ &+ \Delta x_{P_6} \Delta y_{P_6} \frac{\partial^2 f_\alpha^{\mathrm{eq}}(F, t)}{\partial x \partial y} + O[(\Delta x_{P_6})^3, (\Delta y_{P_6})^3] \,, \end{aligned} \tag{14}$$

where $\Delta x_{P_6} = x_{P_6} - (x_P - e_{\alpha x}\delta t)$, $\Delta y_{P_6} = y_{P_6} - (y_P - e_{\alpha y}\delta t)$. For the two-dimensional case, this expansion involves six unknowns, that is, one equilibrium distribution function at point F, two first-order derivatives and three second-order derivatives at this point. To solve these unknowns and avoid using the finite difference to approximate the derivative, six equations are needed to close the system. This can be done by applying the second-order Taylor series expansion at six points: P, P_3, P_4, P_5, P_6, P_7. The following equation system can be obtained

$$f'_k = \{s_k\}^T \{W\} = \sum_{j=1}^{6} s_{k,j} W_j \,, \qquad k = P, P_3, P_4, P_5, P_6, P_7 \,, \tag{15}$$

where

$$\begin{aligned} f'_k &= f_\alpha^{\mathrm{eq}}(x_k, y_k, t) \,, \\ \{s_k\}^T &= \left\{ 1, \Delta x_k, \Delta y_k, \frac{(\Delta x_k)^2}{2}, \frac{(\Delta y_k)^2}{2}, \Delta x_k \Delta y_k \right\} \,, \\ \{W\} &= \left\{ f_\alpha^{\mathrm{eq}}, \frac{\partial f_\alpha^{\mathrm{eq}}}{\partial x}, \frac{\partial f_\alpha^{\mathrm{eq}}}{\partial y}, \frac{\partial^2 f_\alpha^{\mathrm{eq}}}{\partial x^2}, \frac{\partial^2 f_\alpha^{\mathrm{eq}}}{\partial^2 y}, \frac{\partial^2 f_\alpha^{\mathrm{eq}}}{\partial x \partial y} \right\}^T \,. \end{aligned} \tag{16}$$

Our target is to find the first element $W_1 = f_\alpha^{\mathrm{eq}}(F, t)$. Equation (15) can be put into the following matrix form

$$[S]\{W\} = \{f'\} \,, \tag{17}$$

where $[S]$ is a matrix formed by the vector $\{s_k\}$. In practical applications, it was found that the matrix $[S]$ might be singular or ill-conditioned using only six points (P, P_3, P_4, P_5, P_6 and P_7). To overcome this difficulty and make the method more general, more points are used and the least squares approach[10] was introduced to optimize the over-constrained approximation by Eq. (17). As a result, the equation system for $\{W\}$ becomes

$$\{W\} = ([S]^T [S])^{-1} [S]^T \{f'\} = [A]\{f'\} \,. \tag{18}$$

From Eq. (18), we can have

$$f_\alpha^{\mathrm{eq}}(F,t) = W_1 = \sum_{k=0}^{M-1} a_{1,k} f'_k \,, \tag{19}$$

where $a_{1,k}$ are elements of the first row of the matrix $[A]$, which are determined by coordinates of mesh points, the particle velocity and time step size, and will not be changed in the calculation procedure; M is the number of points used and should be greater than 5. In the present study, a structured grid is used and M is taken as 8. This means that for a reference mesh point P, we need to select its eight neighboring points to compute the coefficient in Eq. (19). The above procedure shows the calculation of $f_\alpha^{\mathrm{eq}}(F,t)$ and the same procedure can be applied to calculate the equilibrium density distribution function at other points such as A, B, C and so on. Then the density and velocity can be obtained by:

$$\rho(\mathbf{x}, t+\delta t) = \sum_{A-H} \sum_{k=0}^{M-1} a_{1,k} f'_k, \rho(\mathbf{x}, t+\delta t)\mathbf{V}(\mathbf{x}, t+\delta t) = \sum_{A-H} \sum_{k=0}^{M-1} a_{1,k} f'_k \mathbf{e}_\alpha \,. \tag{20}$$

We can calculate the coefficient in Eq. (20) once and store them in advance, so little computational effort is introduced as compared with the original lattice kinetic scheme. On the other hand, Eq. (20) does not depend on the mesh structure. It only needs the information of coordinates of mesh points. Thus, we can say that Eq. (20) can be consistently used to any kind of mesh structure. But we have to indicate that, as compared to the original lattice kinetic scheme, the present method requires more memory to store the coefficient $a_{1,k}$. This is the price paid for its application to the arbitrary mesh. Equations (3) and (20) form the new lattice kinetic scheme.

2.2.2. *Changing c_s*

Without introducing the derivative term in the equilibrium density distribution function, the kinematic viscosity is written as $\upsilon = (1/2)c_s^2 \delta t$. From this relationship, we can see that the difficulty of the relatively large viscosity can also be coped with changing c_s besides the above-mentioned change of δt. This can be realized by constructing new particle velocity models which have variable c_s. One of this kind of particle velocity models, which is called three-layer 13-bit model in this paper, is proposed by us.

For each layer, the lattice velocities are written as:

$$\mathbf{c}_i^{(m)} = c^{(m)}(\cos\theta_i^{(m)}, \sin\theta_i^{(m)}) \,, \tag{21}$$

$$\theta_i^{(m)} = \theta_0^{(m)} + (i-1)\theta \,, \qquad \theta = \frac{2\pi}{N^{(m)}} \,, \tag{22}$$

where $i = 1, \ldots, N^{(m)}$.

Then the lattice tensors at each layer are expressed as:

$$L_\alpha = \sum_{i=1}^{N} c_{i\alpha}^{(m)} = 0\,, \tag{23}$$

$$L_{\alpha\beta} = \sum_{i=1}^{N} c_{i\alpha}^{(m)} c_{i\beta}^{(m)} = f^{(m)}\delta_{\alpha\beta} = \frac{1}{2} N^{(m)} {c^{(m)}}^2 \delta_{\alpha\beta}\,, \tag{24}$$

$$L_{\alpha\beta\gamma} = \sum_{i=1}^{N} c_{i\alpha}^{(m)} c_{i\beta}^{(m)} c_{i\gamma}^{(m)} = 0\,, \tag{25}$$

$$L_{\alpha\beta\gamma\chi} = \sum_{i=1}^{N} c_{i\alpha}^{(m)} c_{i\beta}^{(m)} c_{i\gamma}^{(m)} c_{i\chi}^{(m)} = g^{(m)}\Delta_{\alpha\beta\gamma\chi} = \frac{N^{(m)}}{8} {c^{(m)}}^4 \Delta_{\alpha\beta\gamma\chi}\,, \tag{26}$$

for any $N^{(m)} \geq 5$ if $\mathbf{c}_i^{(m)} \neq 0$.

Three-layer 13-bit model is used here, which is $m = 0,\ 1,\ 2$; $\mathbf{c}_i^{(0)} = 0$, $N^{(0)} = 1$; $\mathbf{c}_i^{(1)} = c^{(1)}$, $N^{(1)} = 6$ and $\mathbf{c}_i^{(2)} = c^{(2)}$, $N^{(2)} = 6$. For convenience, they are written as:

$$c_i = \begin{cases} 0\,, & i = 0\,, \\ c^{(1)}(\cos\theta_i^{(1)}, \sin\theta_i^{(1)})\,, & i = 1, \ldots, 6\,, \\ c^{(2)}(\cos\theta_i^{(2)}, \sin\theta_i^{(2)})\,, & i = 7, \ldots, 12\,, \end{cases} \tag{27}$$

where

$$\theta_i^{(1)} = \theta_0^{(1)} + (i-1)\theta^{(1)}\,, \qquad \theta^{(1)} = \frac{2\pi}{6} \text{ and } \theta_i^{(2)} = \theta_0^{(2)} + (i-7)\theta^{(2)}\,, \qquad \theta^{(2)} = \frac{2\pi}{6}\,.$$

Their equilibrium density distribution functions are:

$$f_i^{\mathrm{eq}} = \begin{cases} A_0 + D_0\mathbf{u}^2\,, & i = 0\,, \\ A_1 + B_1 c_{i\alpha}u_\alpha + C_1 c_{i\alpha}c_{i\beta}u_\alpha u_\beta + D_1\mathbf{u}^2\,, & i = 1, \ldots, 6\,, \\ A_2 + B_2 c_{i\alpha}u_\alpha + C_2 c_{i\alpha}c_{i\beta}u_\alpha u_\beta + D_2\mathbf{u}^2\,, & i = 7, \ldots, 12\,. \end{cases} \tag{28}$$

In order to recover correct NS equations by Chapman–Enskog expansion, the following constraints have to be satisfied:

$$\sum_m \sum_i A_m = \rho\,, \tag{29a}$$

$$\sum_m C_m f^{(m)} + \sum_m \sum_i D_m = 0\,, \tag{29b}$$

$$\sum_m B_m f^{(m)} = \rho\,, \tag{29c}$$

$$\sum_m A_m f^{(m)} = c_s^2 \rho \,, \tag{29d}$$

$$2\sum_m C_m g^{(m)} = \rho \,, \tag{29e}$$

$$\sum_m (D_m f^{(m)} + C_m g^{(m)}) = 0 \,, \tag{29f}$$

$$\sum_m B_m g^{(m)} = c_s^2 \rho \,, \tag{29g}$$

where

$$f^{(0)} = 0, f^{(1)} = 3\|c^{(1)}\|^2 \,, \qquad f^{(2)} = 3\|c^{(2)}\|^2 \,,$$
$$g^{(0)} = 0 \,, \qquad g^{(1)} = \frac{3}{4}\|c^{(1)}\|^4 \,, \qquad g^{(2)} = \frac{3}{4}\|c^{(2)}\|^4 \,.$$

In order to close the equation system, it is reasonable to choose

$$\frac{A_1}{A_2} = \frac{B_1}{B_2} = \frac{C_1}{C_2} = \frac{D_1}{D_2} = r \,. \tag{30}$$

Solving Eqs. (29) and (30), we can get

$$c_s^2 = \frac{r\|c^{(1)}\|^4 + \|c^{(2)}\|^4}{4r\|c^{(1)}\|^2 + 4\|c^{(2)}\|^2} \,, \tag{31a}$$

$$A_0 = \rho - \frac{2c_s^2\rho(r+1)}{r\|c^{(1)}\|^2 + \|c^{(2)}\|^2} \,, \qquad A_1 = \frac{c_s^2 r\rho}{3(r\|c^{(1)}\|^2 + \|c^{(2)}\|^2)} \,,$$
$$A_2 = \frac{c_s^2\rho}{3(r\|c^{(1)}\|^2 + \|c^{(2)}\|^2)} \,, \tag{31b}$$

$$B_1 = \frac{r\rho}{3(r\|c^{(1)}\|^2 + \|c^{(2)}\|^2)} \,, \qquad B_2 = \frac{\rho}{3(r\|c^{(1)}\|^2 + \|c^{(2)}\|^2)} \,, \tag{31c}$$

$$C_1 = \frac{2r\rho}{3(r\|c^{(1)}\|^4 + \|c^{(2)}\|^4)} \,, \qquad C_2 = \frac{2\rho}{3(r\|c^{(1)}\|^4 + \|c^{(2)}\|^4)} \,, \tag{31d}$$

$$D_0 = -\frac{2\rho(r\|c^{(1)}\|^2 + \|c^{(2)}\|^2)}{r\|c^{(1)}\|^4 + \|c^{(2)}\|^4} + \frac{\rho(r+1)}{r\|c^{(1)}\|^2 + \|c^{(2)}\|^2} \,,$$
$$D_1 = -\frac{1}{2}B_1 \,, \qquad D_2 = -\frac{1}{2}B_2 \,, \tag{31e}$$

$$r = \frac{\|c^{(2)}\|^4 - 4c_s^2\|c^{(2)}\|^2}{4c_s^2\|c^{(1)}\|^2 - \|c^{(1)}\|^4} \,. \tag{31f}$$

In order to make sure that r is positive, the following relationship should be satisfied:

$$\|c^{(1)}\| \leq 2c_s \leq \|c^{(2)}\| \,. \tag{32}$$

Here we suppose that $\|c^{(1)}\| \leq \|c^{(2)}\|$. Then this model can be used to adjust c_s according to the Reynolds number. If a Reynolds number is given, c_s is determined from the relationship $\upsilon = (1/2)c_s^2\delta t$ for a given δt that is determined from the minimum grid spacing of the generated mesh. Then the particle velocities are determined from Eq. (32). In this study, the particle velocities are selected as $\|c^{(1)}\| = 2.0c_s$, $\|c^{(2)}\| = 2.0c_s + 1$, and r is determined according to Eq. (31a). If the particle velocities are determined, the systems (20), (27) and (28) form the new lattice kinetic scheme. We choose $\theta_0^{(1)} = 0$, $\theta_0^{(2)} = 0$ in the following numerical simulations using this new lattice kinetic scheme.

3. Boundary Conditions

On the boundary, usually macroscopic variables and their first order derivative are specified. These conditions can be implemented for the lattice kinetic scheme in the same way as those for the conventional computational fluid dynamics (CFD) methods. This is one of the most attractive advantages of the lattice kinetic scheme over the standard LBM.

4. Numerical Simulations

In order to validate our new lattice kinetic schemes, numerical simulations are carried out. The problem considered is the two-dimensional viscous flow in a square cavity. An incompressible fluid is bounded by a square enclosure and the flow is driven by a uniform translation of the top. The fluid motion generated in this cavity is an example of closed streamline problems that are of theoretical importance because they are part of a broader field of steady, separated flows. The literature on this flow configuration is abundant, which shows rich vortex phenomena at many scales depending on the Reynolds number, Re. Numerical methods for solving Navier–Stokes equations are often tested and evaluated on cavity flows because of the complexity of the flow. They are used here to validate our new lattice kinetic schemes.

The present simulations use nonuniform Cartesian coordinates with the origin located at the lower left corner. The top boundary moves from left to right with velocity U. A typical nonuniform grid is shown in Fig. 2. It can be seen clearly from Fig. 2 that mesh points are stretched near the wall to capture the thin boundary layer. For the first method by changing δt, the minimum grid distance is required to satisfy $6\,\mathrm{Ma/Re}$. For the second method by changing c_s, there is no such requirement. In the middle part of the flow field, the mesh is relatively coarse since velocity gradients are not very large in this region.

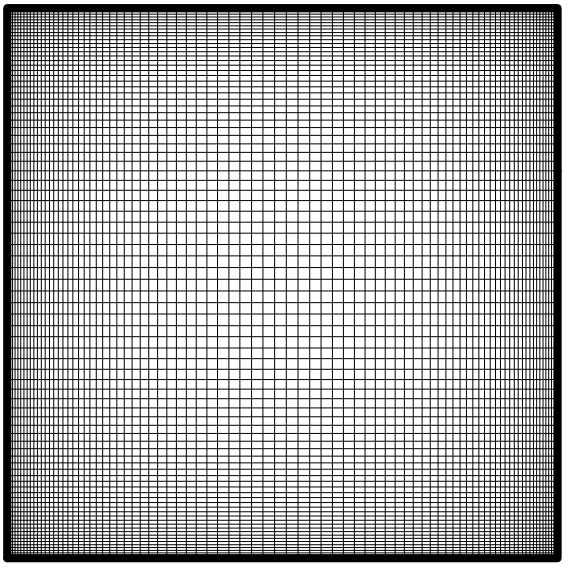

Fig. 2. Typical nonuniform grid.

Numerical simulations were carried out for Re = 100, 400 and 1000. The numerical results are given and discussed below.

4.1. *Flow at* Re = 100

For this low Reynolds number, Ma is chosen to be 0.05. If the uniform grid is used, the grid size has to be 333 in each direction when the first-order derivative is not introduced into the equilibrium density distribution function. The grid size can be reduced by increasing the Mach number. However, this will increase the compressibility error.[11] When the nonuniform grid is used, for the first method, we only need to control the minimum δx or δy to be 0.003, which makes δt be 0.003. This can be easily realized by the grid generation. For the second method, when the nonuniform grid is generated, δt is determined from the minimum grid spacing. Then c_s is determined from $\upsilon = (1/2)c_s^2\delta t$. The new particle velocity model is constructed according to Eqs. (27), (28) and (32).

The simulation results for the center of vortexes at Re = 100 using these two new lattice kinetic schemes are shown in Table 1. The mesh size used is 101×101. The benchmark results of Ghia *et al.*[12] are included for comparison. From this table, it can be seen that our results using the new lattice kinetic schemes are in good agreement with those by Ghia *et al.*[12] The results using the original lattice kinetic scheme by Inamuro[7] on the same mesh size are also included in this table. Our results agree a little better with the benchmark data. Figures 3 and 4 show the velocity components along vertical and horizontal center lines. They agree well with benchmark results.

Table 1. Comparison for locations of vertex centers at Re = 100.

	Changing δt (x, y)	Changing c_s (x, y)	Results of Ghia *et al.*[12] (x, y)	Original scheme (x, y)
Primary	(0.618, 0.738)	(0.619, 0.740)	(0.6172, 0.7344)	(0.619, 0.740)
Left corner	(0.031, 0.038)	(0.033, 0.042)	(0.0313, 0.0391)	(0.027, 0.040)
Right corner	(0.940, 0.059)	(0.943, 0.064)	(0.9453, 0.0625)	(0.940, 0.055)

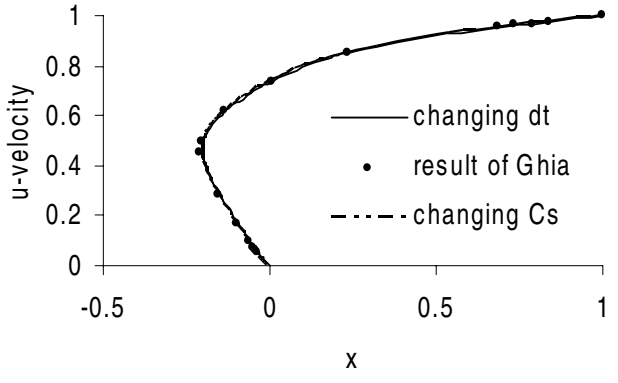

Fig. 3. Comparison of u-velocity profiles along the vertical centerline at Re = 100.

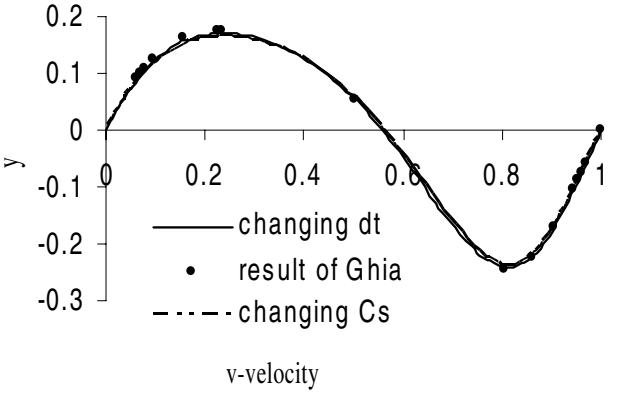

Fig. 4. Comparison of v-velocity profiles along the horizontal centerline at Re = 100.

As far as the computation time is concerned, the calculations are done on Pentium IV 2.4 GHz. The calculation time (seconds) needed for the first lattice kinetic scheme is 2216.14, while the second lattice kinetic scheme needs 3466.61. It takes longer for the second lattice kinetic scheme, since it uses the 13-bit lattice model instead of the 9-bit model.

4.2. *Flow at* Re = 400

For this medium Reynolds number, Ma is chosen to be 0.1. If the uniform grid is used, the grid size has to be 667 in each direction. This large grid size will waste a lot of computational time. If the nonuniform grid is used, for the method by changing δt, we only need to control the minimum δx or δy to be 0.0015, which causes δt to be 0.0015. This can also be easily realized by the grid generation.

The simulation results for the center of vortexes at Re = 400 are shown in Table 2. The mesh size used is 151×151. From this table, we can see that the

Table 2. Comparison for locations of vortex centers at Re = 400.

	Changing δt (x, y)	Changing c_s (x, y)	Results of Ghia *et al.*[12] (x, y)	Original scheme (x, y)
Primary	(0.562, 0.611)	(0.564, 0.614)	(0.5547, 0.6055)	(0.557, 0.608)
Left corner	(0.050, 0.047)	(0.052, 0.048)	(0.0508, 0.0469)	(0.048, 0.049)
Right corner	(0.887, 0.123)	(0.887, 0.124)	(0.8906, 0.1250)	(0.884, 0.123)

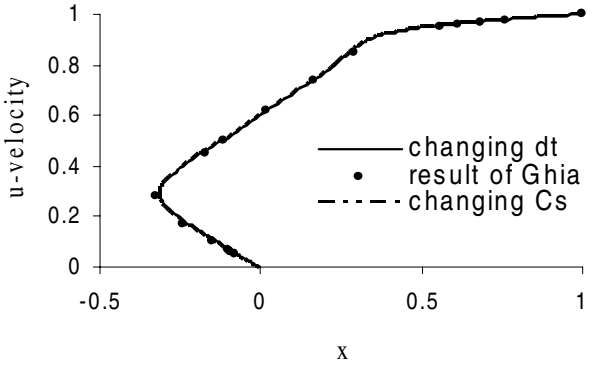

Fig. 5. Comparison of u-velocity profiles along the vertical centerline at Re = 400.

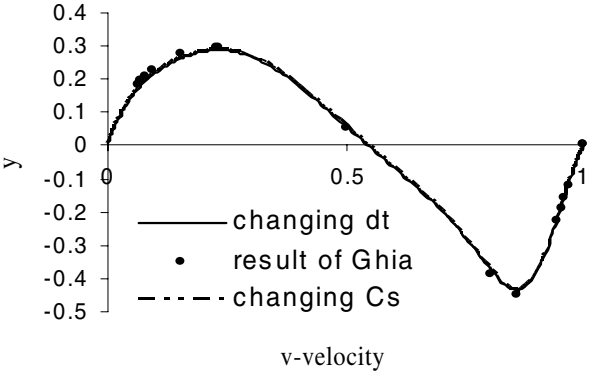

Fig. 6. Comparison of v-velocity profiles along the horizontal centerline at Re = 400.

primary vortex center moves down towards the geometric center of the cavity as the Reynolds number increases. The results are in good agreement with those by Ghia *et al.*[12] Compared with the result using the original lattice kinetic scheme, our results agree a little better with the benchmark data. Figures 5 and 6 show the velocity components along vertical and horizontal center lines. They agree well with benchmark data. From these two figures, we can see that in the central core of the cavity, velocity profiles change from curved to linear as the Reynolds number increases from 100 to 400. These agree well with the vorticity contour, which will be shown in the following.

4.3. *Flow* Re = 1000

For this high Reynolds number, Ma is chosen to be 0.15. If the uniform grid is used, the grid size has to be 1111 in each direction. This large grid size is time consuming and requires large amounts of computer memory for the numerical simulation. However, when the nonuniform grid is used, for the first method, we only need to make sure that the minimum δx or δy to be 0.0009, which makes δt be 0.0009. This is not difficult to be realized by using the highly stretched grid near the wall.

The calculation results for the center of vortexes at Re = 1000 are shown in Table 3. The mesh size is 251×251. As seen from this table, the primary vortex center moves further down towards the geometric center of the cavity. The results are in good agreement with those by Ghia *et al.*[12] and they are a little better than

Table 3. Comparison for locations of vortex centers at Re = 1000.

	Changing δt (x, y)	Changing c_s (x, y)	Results of Ghia *et al.*[12] (x, y)	Original scheme (x, y)
Primary	(0.528, 0.563)	(0.534, 0.567)	(0.5313, 0.5625)	(0.532, 0.569)
Left corner	(0.082, 0.076)	(0.083, 0.076)	(0.0859, 0.0781)	(0.081, 0.076)
Right corner	(0.864, 0.113)	(0.867, 0.113)	(0.8594, 0.1094)	(0.868, 0.114)

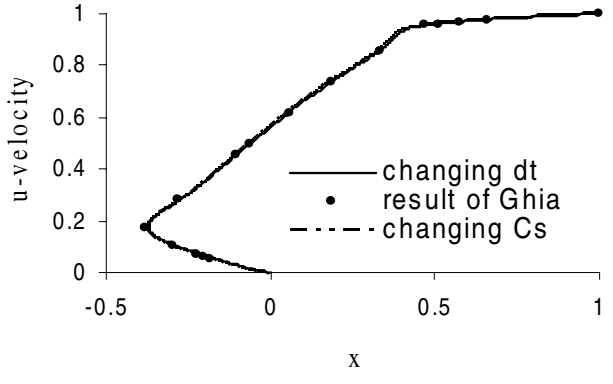

Fig. 7. Comparison of u-velocity profile along the vertical centerline at Re = 1000.

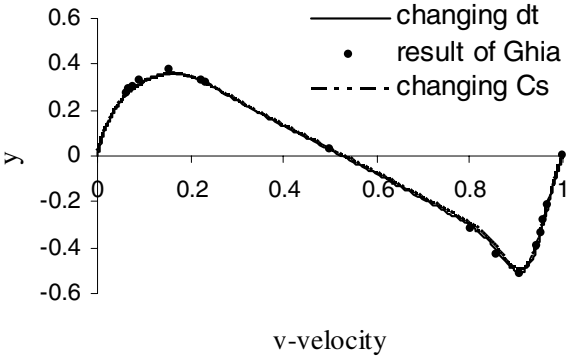

Fig. 8. Comparison of v-velocity profiles along the horizontal centerline at Re = 1000.

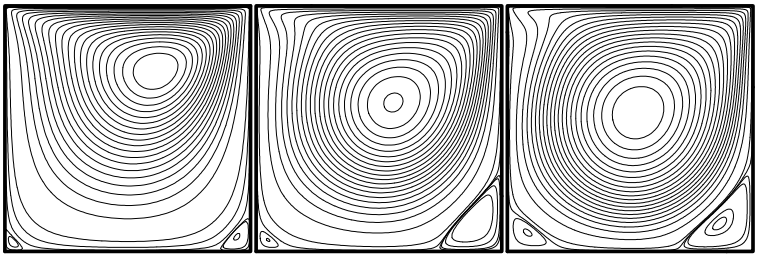

Fig. 9. Streamlines for driven cavity flow at Re = 100, 400 and 1000.

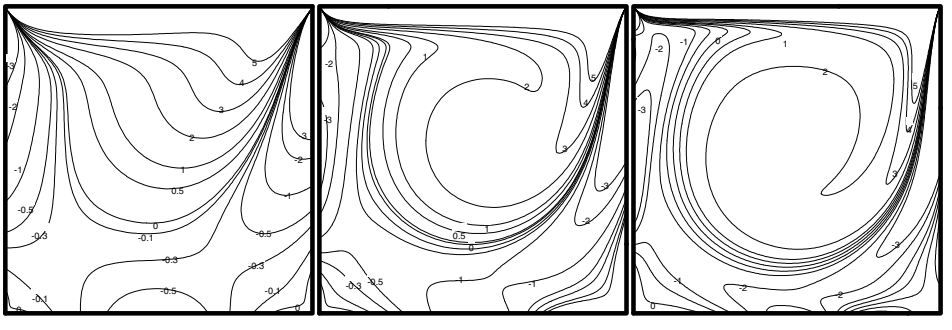

Fig. 10. Vorticity contour for driven cavity flow at Re = 100, 400 and 1000.

those using the original lattice kinetic scheme. Figures 7 and 8 show the velocity components along vertical and horizontal center lines. Again, they agree well with benchmark data. It can be seen from these two figures that, in the central core of the cavity, velocity profiles become more linear as the Reynolds number increases from 400 to 1000.

Figures 9 and 10 show the streamline and vorticity contour for Reynolds numbers of 100, 400 and 1000. It is noted that both lattice kinetic schemes proposed

in this work provide the same streamline and vorticity contour. It is observed from the vorticity contour that, as the Reynolds number increases to 400, there exists a central, inviscid core of nearly constant vorticity with viscous effects confined to the thin shear layer near the walls. As it increases to 1000, the central, inviscid core of nearly constant vorticity becomes larger than that at Re = 400. This effect is well reflected on the velocity component profile.

5. Conclusions

New lattice kinetic schemes which are based on the original lattice kinetic scheme by Inamuro are proposed in this work. We found that in the original lattice kinetic scheme, there is a first-order derivative term in the equilibrium density distribution function which makes it more complicated as compared to that used by the conventional LBM. The finite difference approximation of these derivatives will cause the numerical error, especially at a high Reynolds number, this may lead to numerical instability. When this original lattice kinetic scheme was extended to be used on the arbitrary mesh by introducing the Taylor series expansion and least squares approximation techniques, we found that there is no need to introduce the first-order derivative term. The difficulty of the relatively large viscosity on uniform grids can be eased by controlling δt. Therefore, the new lattice kinetic scheme by changing δt is proposed. From the relationship of $\upsilon = (1/2)c_s^2\delta t$, we found that besides changing δt, we can ease the problem of the relatively large viscosity by changing c_s. This is realized by proposing the new particle velocity model which has variable c_s. This is the second new lattice kinetic scheme. Numerical results of the two-dimensional square driven cavity flow for Reynolds numbers of 100 to 1000 validate the new lattice kinetic schemes.

References

1. S. Chen and G. D. Doolen, *Annu. Rev. Fluid Mech.* **30**, 329 (1998).
2. D. d'Humieres, *Rarefied Gas Dynamics*: *Theory and Simulations*, eds. B. D. Shizgal and D. P. Weaver, Progress in Astronautics and Aeronautics, Vol. 159 (AIAA, Washington DC, 1992), pp. 450–458.
3. P. Lallemand and L.-S. Luo, *Phys. Rev. E* **61**, 6546 (2002).
4. R. Cornubert, D. d'Humieres and D. Levermore, *Physica D* **47**, 241 (1991).
5. D. P. Ziegler, *J. Stat. Phys.* **71**, 1171 (1993).
6. S. Chen, D. Martinez and R. Mei, *Phys. Fluids* **8**, 2527 (1996).
7. T. Inamuro, *Phil. Trans. R. Soc. Lond. A* **360**, 477 (2002).
8. Y. Peng, C. Shu and Y. T. Chew, *Phys. Rev. E* **69**, 016703 (2004).
9. S. Succi, *The Lattice Boltzmann Equation for Fluid Dynamics and Beyond*, Chap. 4 (Oxford University Press, 2001), pp. 62–63.
10. G. H. Golub and C. F. Van Loan, *Matrix Computations*, 3rd edn. (Johns Hopkins University Press, 1996).
11. S. Hou, Q. Zou, G. Doolen and A. Cogley, *J. Comput. Phys.* **118**, 329 (1995).
12. U. Ghia, K. N. Ghia and C. T. Shin, *J. Comput. Phys.* **48**, 387 (1982).